

Multibeam and Beam Scanning With Modulated Metasurfaces

Modeste Bodehou¹, *Student Member, IEEE*, Enrica Martini², *Senior Member, IEEE*,
Stefano Maci, *Fellow, IEEE*, Isabelle Huynen¹, *Senior Member, IEEE*,
and Christophe Craeye¹, *Senior Member, IEEE*

Abstract—Multibeam and beam-scanning capabilities of metasurface (MTS) antennas using multiple feeds are investigated. The MTS synthesis is performed by direct inversion of an electric field integral equation (EFIE) obtained after expanding the unknown equivalent impedance profile into Fourier-Bessel basis functions. Two approaches are explored. The first one assumes *a priori* a discrete azimuthal symmetry in the impedance profile, so as to constrain the solution to a subspace which automatically provides multiple beams when illuminated with feeds regularly arranged along azimuth. In the second approach, there are not *a priori* assumptions on the impedance profile, but the systems of equations corresponding to each beam are stacked and solved simultaneously in the least-squares sense. This second approach can also be used to obtain polarization diversity. More importantly, it also enables continuous beam scanning. The latter functionality is achieved through the generation of two embedded patterns in a common azimuthal window with opposite phase slopes, followed by a continuous phasing of the two feed points. Various designs are presented in this article. All the results are validated with the method of moments (MoM).

Index Terms—Basis functions, beam scanning, impedance boundary condition (IBC), leaky-wave (LW) antennas, metasurfaces (MTSs), multibeams.

I. INTRODUCTION

APERTURE antennas with multibeam and beam-scanning capabilities are required in several applications, including radar [1]–[3], terrestrial [4]–[7] and satellite [8], [9] communications, and radio astronomy [10]–[12]. In general, beam reconfigurability is obtained by changing the antenna properties electrically, optically, mechanically, or using a tunable material (such as liquid crystal) [13]. Metasurface (MTS) antennas have emerged in the last few years as a new class of

Manuscript received May 3, 2019; revised July 26, 2019; accepted August 4, 2019. Date of publication October 4, 2019; date of current version March 3, 2020. This work was supported by the Fonds pour la formation à la Recherche dans l’Industrie et dans l’Agriculture (FRIA) grant through the Belgium Fonds National de la Recherche Scientifique (FNRS). (*Corresponding author: Modeste Bodehou.*)

M. Bodehou, I. Huynen, and C. Craeye are with the Institute of Information and Communication Technologies, Electronics and Applied Mathematics (ICTEAM), Université catholique de Louvain, 1348 Louvain-la-Neuve, Belgium (e-mail: modeste.bodehou@uclouvain.be; isabelle.huynen@uclouvain.be; christophe.craeye@uclouvain.be).

E. Martini and S. Maci are with the Department of Information Engineering and Mathematics, University of Siena, 53100 Siena, Italy (e-mail: martini@dii.unisi.it; macis@dii.unisi.it).

Color versions of one or more of the figures in this article are available online at <http://ieeexplore.ieee.org>.

Digital Object Identifier 10.1109/TAP.2019.2944554

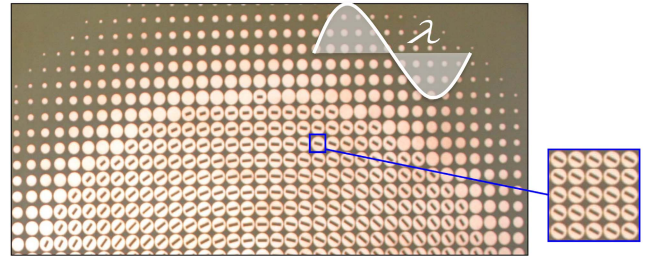


Fig. 1. Illustration of a surface impedance implemented with sub-wavelength patches, assuming a local periodicity.

leaky-wave (LW) antennas with a unique pattern shaping capability [14]–[21]. This characteristic makes them intrinsically amenable to reconfigurability. Furthermore, those antennas are low profile by essence, since the basic mechanism relies on the perturbation of a surface-wave [22] excited by a coplanar feed on a planar and very thin substrate. MTS antennas also exhibit very low power losses and can be easily manufactured with standard PCB techniques [15], [16]. In practice, those antennas implement a spatially varying surface impedance by means of sub-wavelength scatterers. The surface impedance, thus, describes the MTS in the homogenized limit. Such impedance should be tensorial (also denoted as anisotropic) to allow a better control of the antenna polarization and anti-Hermitian to avoid losses in the antenna [15]. The implementation of the impedance boundary condition (IBC) is usually carried out with a dense array of sub-wavelength patches printed on a substrate, considering a local-periodicity approximation (see an illustration in Fig. 1).

Recently, González-Ovejero *et al.* [23] also demonstrated the alternative of implementing the MTS IBC using metal only, thus avoiding possible losses that can appear in the substrate, especially at high frequency. This article is not dealing with the IBC implementation process, which has been already treated in several publications [24]–[26]. The focus here is put on the IBC synthesis. Generation of multiple beams using an MTS antenna fed at multiple points has already been demonstrated in [27], where it has been shown that assuming a certain orthogonality between the beams, the required modulated impedance corresponding to each excitation can be superimposed. Each impedance modulation is computed analytically based on the flat optics theory proposed in [28].

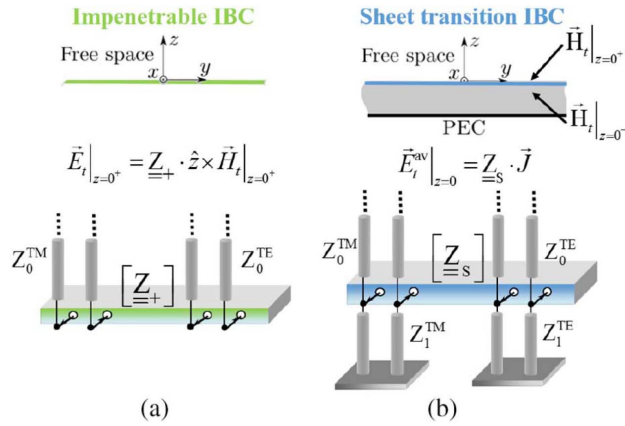


Fig. 2. Equivalent transmission line circuits for (a) impenetrable (opaque) IBC and (b) sheet transition IBC [30].

The first goal of this article consists in extending the synthesis of multiple beam MTS antennas with multiple feeds to shaped beams, which are here not necessarily orthogonal. The methods proposed are built on the synthesis technique described in [20]. This technique relies on the direct inversion of the electric field integral equation (EFIE) after expanding the surface currents, as well as the sheet impedance, in terms of Fourier-Bessel basis functions (FBBFs). In this article, multiple beams are created either by exploiting, when available, the symmetry among objective patterns or stacking the equations corresponding to each beam. This also allows, as a particular case, the generation of two radiation patterns with the same amplitudes and polarizations but with opposite phase slopes. A proper phasing of the feeds then allows continuous beam steering over an angular range equal to the 3 dB beamwidth. Another particular case leads to the generation of two beams with different polarizations.

The manuscript is organized as follows. Section II formulates the problem, introduces the MTS model, and recalls the FBBFs as well as the fundamentals of the EFIE-based synthesis. Section III presents two techniques allowing the design of multifed, multibeam antennas. Section IV presents the numerical results, including the synthesis of an MTS antenna, capable of azimuthal scanning within a limited sector. Finally, Section V concludes this article.

II. PROBLEM FORMULATION

A. MTS Modeling

The antenna we are considering consists of a modulated MTS of circular shape, realized through a distribution of metallic patches over a grounded slab. It is known that a generic MTS containing a ground plane can be described through an impenetrable (opaque) equivalent impedance [see Fig. 2(a)]. However, for the MTSs considered in this article, a more accurate model is provided by the penetrable (transparent) equivalent impedance [24]. Accordingly, the MTS is described by a two-port sheet impedance in parallel with a transmission line network [29], [30], which takes into account the substrate effect [see Fig. 2(b)]. The sheet impedance is defined as the ratio between the averaged

electric field \mathbf{E}_t and the surface current \mathbf{J} on the MTS aperture. The latter represents the jump discontinuity of the magnetic field at the sheet

$$\mathbf{E}_t = \underline{\underline{Z}}_S \cdot \hat{\mathbf{z}} \times (\mathbf{H}_t|_{z=0^+} - \mathbf{H}_t|_{z=0^-}) = \underline{\underline{Z}}_S \cdot \mathbf{J}. \quad (1)$$

In the following, we will assume the absence of losses; therefore, the impedance tensor in (1) is anti-Hermitian. The MTS is fed by a number of coplanar sources described as vertical elementary electric dipoles. The objective here is to determine the impedance modulation required to provide the desired radiation patterns for given positions of the sources. A general approach capable of providing arbitrary radiation pattern for the case of a single central source was recently presented in [20]. This approach is briefly summarized in the following section.

B. MTS Synthesis Through Fourier-Bessel (Basis Functions) Expansion

As already mentioned, MTS antennas are usually built on a circular domain, which suggests the usage of entire-domain basis functions for the EFIE discretization. FBBFs have been proposed in [31] for the current discretization and further used in [20] for the MTS impedance discretization. Those basis functions are defined on a circular domain of radius a as follows [31], [32]:

$$R_{m,n}(\boldsymbol{\rho}) = J_n\left(\lambda_{nm} \frac{\rho}{a}\right) e^{-jn\phi} \quad (2)$$

where λ_{nm} is the m th positive zero of the first-kind Bessel function of order n . The vector $\boldsymbol{\rho} = (\rho, \phi)$ identifies each observation point on the MTS, with ρ and ϕ being the usual polar coordinates. Accordingly, the current distribution is discretized into FBBFs as follows:

$$\mathbf{J}(\boldsymbol{\rho}) = \sum_{n=-N}^N \sum_{m=1}^M i_{mn}^\rho R_{m,n}^\rho(\boldsymbol{\rho}) \hat{\boldsymbol{\rho}} + i_{mn}^\phi R_{m,n}^\phi(\boldsymbol{\rho}) \hat{\boldsymbol{\phi}} \quad (3)$$

where $\hat{\boldsymbol{\rho}}$ and $\hat{\boldsymbol{\phi}}$ are the unit vectors along the radial and azimuthal directions, respectively. The entries in polar coordinates of the tensorial impedance is now assumed to be of the following form:

$$\begin{aligned} Z_S^{\rho\rho}(\boldsymbol{\rho}) &= Z_0^{\rho\rho} + P^{\rho\rho}(\boldsymbol{\rho}) \\ Z_S^{\rho\phi}(\boldsymbol{\rho}) &= -(Z_S^{\phi\rho}(\boldsymbol{\rho}))^* = P^{\rho\phi}(\boldsymbol{\rho}) \\ Z_S^{\phi\phi}(\boldsymbol{\rho}) &= Z_0^{\phi\phi} - P^{\rho\rho}(\boldsymbol{\rho}) \end{aligned} \quad (4)$$

where $Z_0^{\rho\rho}$ and $Z_0^{\phi\phi}$ are the average impedances, which are assumed uniform over the surface. $P^{\rho\rho}$ and $P^{\rho\phi}$ are the impedance modulations to be synthesized. Similar to the currents, the IBC is expanded into FBBFs as follows:

$$Z_S^{\rho\rho}(\boldsymbol{\rho}) \approx \sum_{n_S=-N_S}^{N_S} \sum_{m_S=1}^{M_S} [K_S^{\rho\rho} + X_S^{\rho\rho}] R_{m_S,n_S}(\boldsymbol{\rho}) \quad (5)$$

$$Z_S^{\rho\phi}(\boldsymbol{\rho}) \approx \sum_{n_S=-N_S}^{N_S} \sum_{m_S=1}^{M_S} X_S^{\rho\phi} R_{m_S,n_S}(\boldsymbol{\rho}) \quad (6)$$

$$Z_S^{\phi\phi}(\boldsymbol{\rho}) \approx \sum_{n_S=-N_S}^{N_S} \sum_{m_S=1}^{M_S} [K_S^{\phi\phi} - X_S^{\rho\rho}] R_{m_S,n_S}(\boldsymbol{\rho}) \quad (7)$$

where $K_S^{\rho\rho}$ and $K_S^{\phi\phi}$ are the expansion coefficients of the average impedances $Z_0^{\rho\rho}$ and $Z_0^{\phi\phi}$, respectively. $X_S^{\rho\rho}$ and $X_S^{\rho\phi}$ are the expansion coefficients of the modulation terms $P^{\rho\rho}$ and $P^{\rho\phi}$, respectively. These coefficients are implicitly assumed to depend on m_S and n_S . Since we are looking for an anti-Hermitian IBC, the surface impedance modulation should be purely imaginary, which implies that the coefficients $X_S^{\rho\rho}$ and $X_S^{\rho\phi}$ (which depend on indices n_S and m_S) used for the expansion of the modulated IBC in FBBF should satisfy the following symmetry:

$$(X_S(m_S, -n_S))^* = -(-1)^{n_S} X_S(m_S, n_S). \quad (8)$$

The EFIE discretization with FBBFs leads to a system of equations, which can be written in compact form as follows:

$$\underline{\underline{Z}}^S \underline{\underline{X}}_S = \underline{\underline{U}} \quad (9)$$

where $\underline{\underline{X}}_S$ is the vector representing the unknown coefficients of the impedance modulation, $\underline{\underline{U}}$ contains information regarding the substrate, the excitation as well as the desired radiation pattern, and $\underline{\underline{Z}}^S$ also contains information about the radiation pattern. It is worth noting that, although the solution of the problem leads to the resolution of a linear system of equations, it does not mean that the radiation pattern or the currents depend linearly on the impedance. Indeed, the currents appear in $\underline{\underline{U}}$ and in $\underline{\underline{Z}}^S$ in such a way that there is no linear link between them and $\underline{\underline{X}}_S$. The reader is referred to [20] for the mathematical details behind the formulation and to [21] for the extension of the method to elliptical apertures. In the remainder of this article, we identify basis functions for surface impedance, currents, and testing functions with subscripts S , b , and t , respectively.

III. SYNTHESIS FOR MULTIFED MTS ANTENNA

We want now to generalize the formulation summarized in Section II-B to the case of multiple beams and multiple feeds. Two different approaches are presented in the following. In all the cases, the desired radiation patterns are assumed to be of the general form $\mathbf{F}(\theta, \phi)$, where θ and ϕ are the elevation and azimuthal angles, respectively. It is provided through its transverse magnetic (TM) and transverse electric, (TE) field components w.r.t. z , with electric field parallel to the vectors $\hat{\theta}$, $\hat{\phi}$, respectively (see an illustration in Fig. 3).

A. Synthesis Based on Azimuthal Symmetry Assumption

Let us assume that we want to generate multishaped beams $\mathbf{F}_1(\theta, \phi)$, $\mathbf{F}_2(\theta, \phi)$, \dots , $\mathbf{F}_Q(\theta, \phi)$ satisfying the following symmetry $\mathbf{F}_i(\theta, \phi) = \mathbf{F}_i(\theta, \phi - 2\pi(i-1)/Q)$, $i = 1 \dots Q$. Let us now suppose that the MTS is designed to radiate the beam $\mathbf{F}_1(\theta, \phi)$ when excited at the point $\boldsymbol{\rho}_1 = (\rho_1, \phi_1)$, with $\rho_1 > 0$. One can easily show that, if the modulation satisfies the same symmetry as the beams, namely

$$\underline{\underline{Z}}_S(\rho, \phi) = \underline{\underline{Z}}_S(\rho, \phi - 2\pi(i-1)/Q), \quad i = 1 \dots Q \quad (10)$$

then the MTS automatically radiates the beam $\mathbf{F}_i(\theta, \phi)$ when excited at the point $\boldsymbol{\rho}_i = (\rho_1, \phi_1 + 2\pi(i-1)/Q)$. Since the MTS IBC is discretized into FBBFs, the azimuthal symmetry (10) can be imposed by simply restricting the set of

FBBFs to those with azimuthal index n_S multiple of Q . We want to stress that for higher values of Q , the subspace in which the modulated impedance is designed is smaller [see expressions (5)–(7)]. The algebraic system to be solved has $4M_t(2N_t + 1)$ equations with $2M_S(2(N_S/Q) + 1)$ unknowns, where it has been implicitly assumed that N_S is multiple of Q . This means that the capabilities of shaping the beams, the aperture efficiency, and the computation time decrease for increasing Q . It is important to mention that for stability reasons of the method, one cannot use more basis functions for the impedance than for the currents (i.e., $N_S \leq N_b = N_t$ and $M_S \leq M_b = M_t$).

B. Equations Stacking

The second approach consists of over-constraining the system of equations. Since each system of equations corresponds to a given excitation and a given radiation pattern, one can simply simultaneously impose more equations to achieve the multibeam effect. The system of equations to be solved takes the same form as in (9), with $\underline{\underline{Z}}^S$ and $\underline{\underline{U}}$ written as, respectively,

$$\underline{\underline{Z}}^S = \left[\underline{\underline{Z}}_1^S; \underline{\underline{Z}}_2^S; \dots; \underline{\underline{Z}}_Q^S \right] \quad (11)$$

$$\underline{\underline{U}} = \left[\underline{\underline{U}}_1; \underline{\underline{U}}_2; \dots; \underline{\underline{U}}_Q \right]. \quad (12)$$

Each index corresponds to a given radiation pattern and a given excitation. Matrix $\underline{\underline{Z}}^S$ in (11) has the same number of columns as the one in (9) for the single feed synthesis, which means that we are using the same number of FBBFs for the IBC expansion in both cases (single feed and multiple feeds). This method can deal with more general multibeam configuration with respect to the approach presented in Section III-A. However, one needs to solve a system of $4QM_t(2N_t + 1)$ equations with $2M_S(2N_S + 1)$ unknowns, which means that the size increases with the number of beams Q . Notice that it is essential to add to the visible part of the current spectrum an invisible part corresponding to the exciting surface wave. Omitting that part may significantly worsen the performance and generally yields non-realizable impedance values. The invisible current spectrum, which corresponds to the antenna near-field, is estimated from a simulation of the currents obtained with the average reactance [20] with each feed. However, one can iterate starting from this first estimation. This means that a first impedance modulation can be computed and then used to update the invisible current for each feed. The results obtained with such a refinement are shown in Section IV-B.

For both methods (based on symmetry and equation stacking), the physical degrees of freedom offered by an MTS of given size may become insufficient when the number of desired simultaneous beams is increased. This is expressed in terms of an over-constrained system of equations and explains how the obtained patterns performance may stay behind the requirements when more beams are demanded, as will be shown in Section IV.

IV. NUMERICAL RESULTS

This section presents some examples of application of the multibeam synthesis techniques discussed in Sections III-A and III-B. The IBC design is validated with the

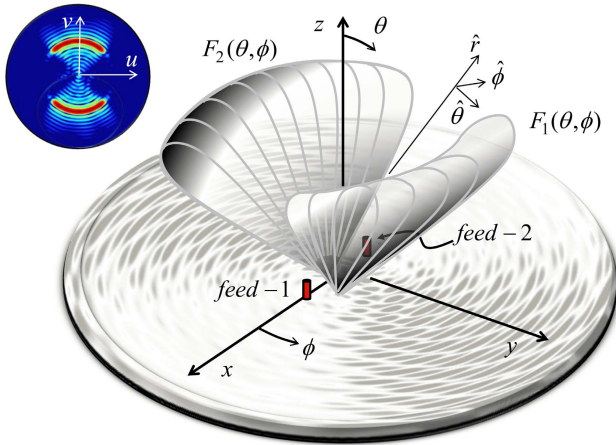


Fig. 3. Circularly polarized azimuthal bi-symmetric radiation pattern.

method of moments (MoM) code presented in [31] and [33]. The chosen frequency of operation is 24 GHz. The substrate's relative permittivity is $\epsilon_r = 3.66$ with a thickness $d = 1.52$ mm. The antenna radius is fixed to $a = 10 \lambda$, with λ being the free-space wavelength. Finally, the average reactance is $X_0^{pp} = X_0^{\phi\phi} = -1260 \Omega$.

A. Multiple Flat Beam Design

In the first example, the MTS is designed to radiate a flat circularly polarized azimuthal beam in the direction $\theta = 30^\circ$ and ϕ in the range between $\phi_1 = 45^\circ$ and $\phi_2 = 135^\circ$ when it is fed with a vertical elementary dipole placed at $(x = 1.5 \lambda, y = 0, z = -d/2)$. The radiation pattern can then be written as $F_{TE} = \cos \phi - j \sin \phi$ and $F_{TM} = \sin \phi + j \cos \phi$ in the targeted direction. The impedance is designed to exhibit a bi-symmetric pattern ($Q = 2$), which means that the antenna should also automatically radiate a flat beam at $\theta = 30^\circ$ and $\phi \in [225^\circ, 315^\circ]$ when fed by a source placed at $(x = -1.5 \lambda, y = 0, z = -d/2)$. We used for the impedance discretization $M_S = 50$, $N_S = 20$. The desired radiation pattern is represented in Fig. 3. This desired radiation pattern is obtained by adding to the ideal visible current distribution (linked to the radiation pattern), the invisible current distribution obtained with the average impedance (as explained in [20]), and by discretizing the overall current with FBBFs. The obtained impedance modulation and the corresponding simulated radiation pattern are depicted in Figs. 4 and 5(a)–(c), respectively. In Fig. 4, as well as in the remainder of this article, dots represent the position of the feeds, while arrows point toward the central part of the beam in the azimuthal plane.

We obtained an average directivity of 21.5 dBi, which corresponds to 49% of the power density of the desired radiation pattern. The same design has now been carried out with the second approach (described in Section III-B). The obtained reactance and the radiation pattern are represented in Figs. 6 and 7, respectively.

A cut of this radiation pattern, as well as a comparison with the results obtained using the symmetry technique (see Section III-A), is illustrated in Fig. 8. One can see

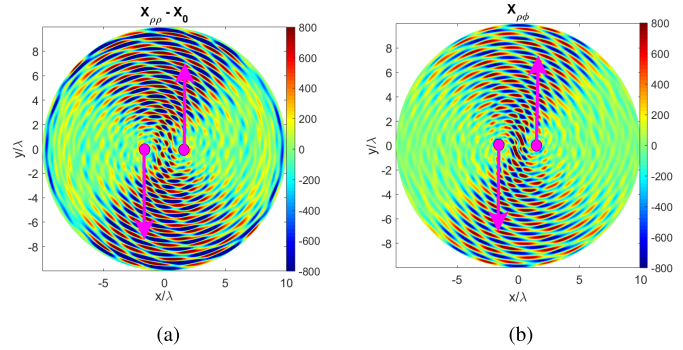


Fig. 4. Modulated sheet impedance for an MTS antenna radiating two symmetric azimuthal beams at $\theta = 30^\circ$ and $\phi \in [45^\circ, 135^\circ]$ and $[225^\circ, 315^\circ]$. Dots represent the position of the point sources and arrows the direction of the central part of the beam in the azimuthal plane (see also Fig. 3). The synthesis is based on the method described in Section III-A. (a) $X_{pp} - X_0$. (b) $X_{\rho\phi}$.

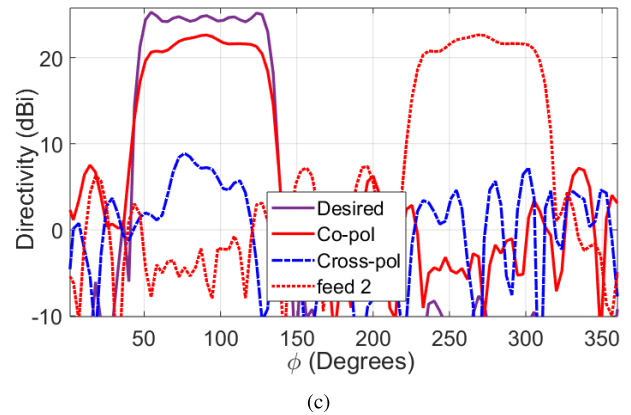
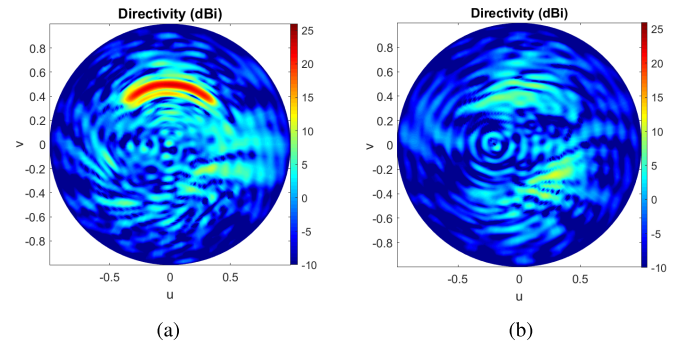


Fig. 5. Circularly polarized azimuthal radiation pattern in the (u, v) plane. (a) Copolar component for the designed MTS. (b) Cross-polar component for the designed MTS. (c) Cut of the radiation pattern along the cone $\theta = 30^\circ$.

that both methods essentially yield the same performance. However, the second approach is much more time and memory consuming than the first one, since the system of equations matrix to solve is four times larger. One can also observe from Figs. 6 and 4 that the modulations are quite similar. However, the MTS aperture is not entirely used, which means that one could add more functionalities by exploiting the less modulated part of the aperture.

In the next example, we compare the results obtained with $Q = 1$, $Q = 2$, and $Q = 3$. For the case $Q = 1$, the source is located at $(x = 1.5 \lambda, y = 0, z = -d/2)$. For the case $Q = 3$,

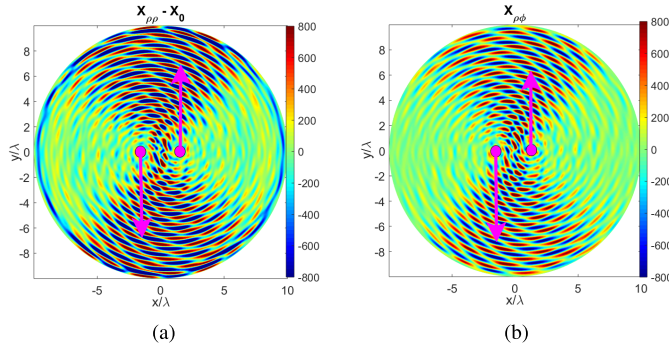


Fig. 6. Modulated sheet impedance for an MTS antenna radiating two symmetric azimuthal beams at $\theta = 30^\circ$ and $\phi \in [45^\circ, 135^\circ]$ and $[225^\circ, 315^\circ]$. Dots represent the position of the point sources and arrows the direction of the central part of the beam in the azimuthal plane. The synthesis is based on the method described in Section III-B. (a) $X_{\rho\rho} - X_0$. (b) $X_{\rho\phi}$.

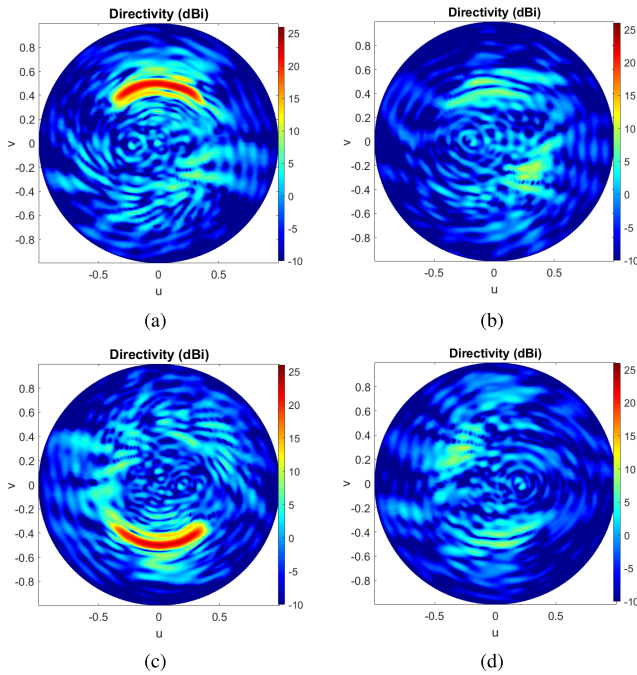
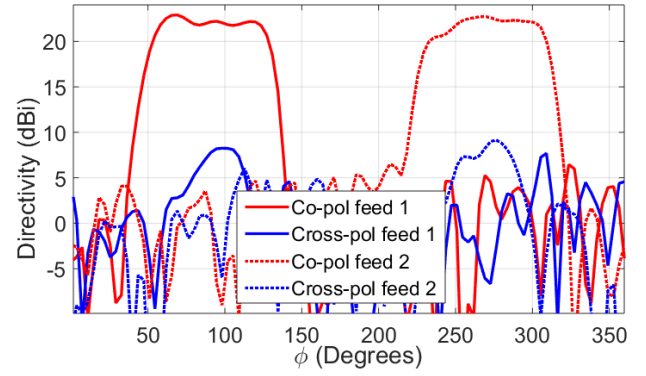


Fig. 7. Circularly polarized azimuthal radiation pattern in the (u, v) plane based on the method of Section III-B. (a) Copolar component when the MTS is fed at $(x = 1.5\lambda, y = 0)$. (b) Cross-polar component when the MTS is fed at $(x = 1.5\lambda, y = 0)$. (c) Copolar component when the MTS is fed at $(x = -1.5\lambda, y = 0)$. (d) Cross-polar component when the MTS is fed at $(x = -1.5\lambda, y = 0)$.

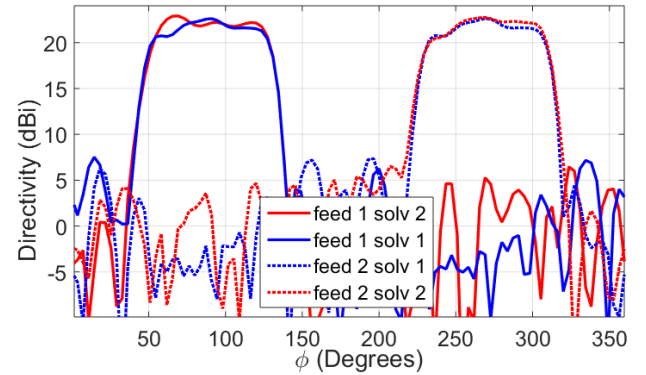
the sources are located at $(x = 1.5\lambda, y = 0, z = -d/2)$, $(x = -0.75\lambda, y = (3\sqrt{3}/4)\lambda, z = -d/2)$, and $(x = -0.75\lambda, y = -3\sqrt{3}/4\lambda, z = -d/2)$. The desired radiation pattern for the case $Q = 3$ is illustrated in Fig. 9. The modulations computed for the cases $Q = 1$ and $Q = 3$ are shown in Fig. 10. As can be seen, the case $Q = 3$ uses more efficiently the aperture. The corresponding radiation patterns are compared in Fig. 11. As expected, the performance decreases when the number of beams increases.

B. Dual Polarization Design

Next, we design an MTS antenna capable of radiating two beams with the same amplitude but with opposite polarizations. Depending on the excited feed, one can select



(a)



(b)

Fig. 8. Cut of the radiation pattern along the cone $\theta = 30^\circ$ for an MTS radiating an azimuthal bi-symmetric radiation pattern. (a) Results from the method described in Section III-B. (b) Comparison between the results with the method in Section III-A (solv 1) and the one in Section III-B (solv 2).

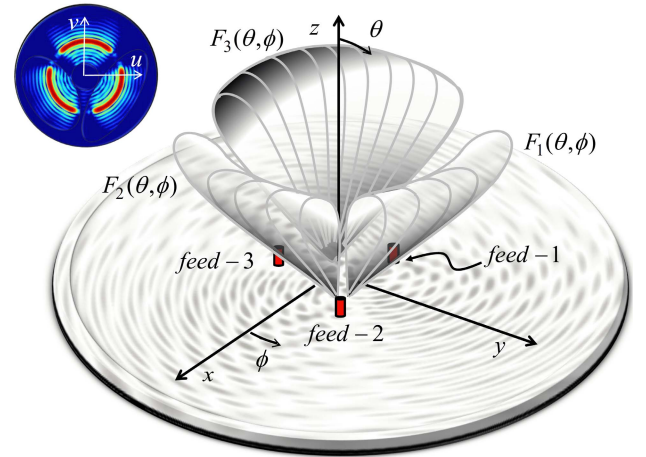


Fig. 9. Circularly polarized azimuthal tri-symmetric radiation pattern.

a given polarization. A similar functionality has recently been proposed in [34] using holographic techniques. Here, we feed the MTS as in Section IV-A. The IBC is designed in such a way to provide for the first excitation, located at $(x = 1.5\lambda, y = 0, z = -d/2)$, a flat right-handed circularly polarized (RHCP) radiation pattern in the sector $(\theta = 30^\circ$ and $\phi \in [67.5^\circ, 112.5^\circ])$. When the MTS is excited with the second feed, located at $(x = -1.5\lambda, y = 0, z = -d/2)$, the antenna should radiate a flat left-handed circularly polarized (LHCP) radiation pattern in the same sector as for the

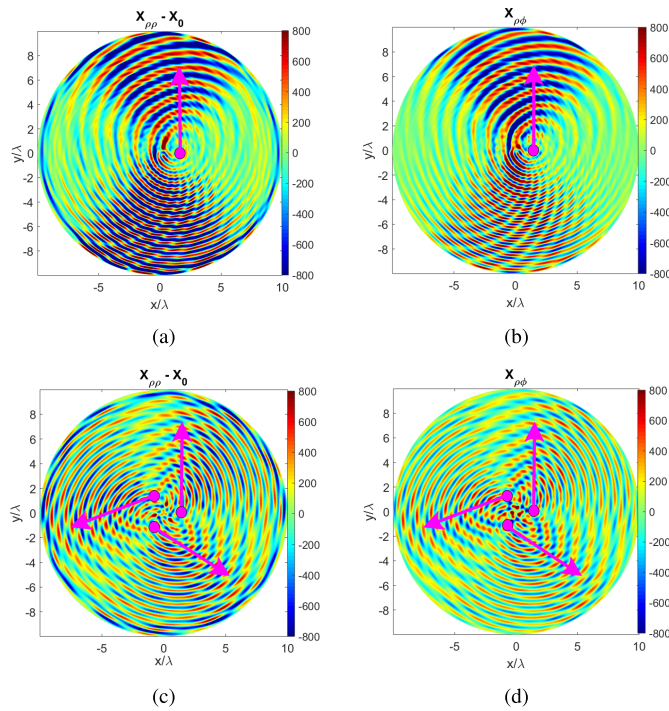


Fig. 10. Modulated sheet impedance for an MTS antenna radiating azimuthal beams at $\theta = 30^\circ$ based on the method described in Section III-A. (a) $X_{\rho\rho} - X_0$ for a nonsymmetric beam ($Q = 1$). (b) $X_{\rho\phi}$ for a nonsymmetric beam ($Q = 1$). (c) $X_{\rho\rho} - X_0$ for a tri-symmetric beam ($Q = 3$). (d) $X_{\rho\phi}$ for a tri-symmetric beam ($Q = 3$). Dots represent the position of the point sources and arrows the direction of the central part of the beam in the azimuthal plane (see also Fig. 9).

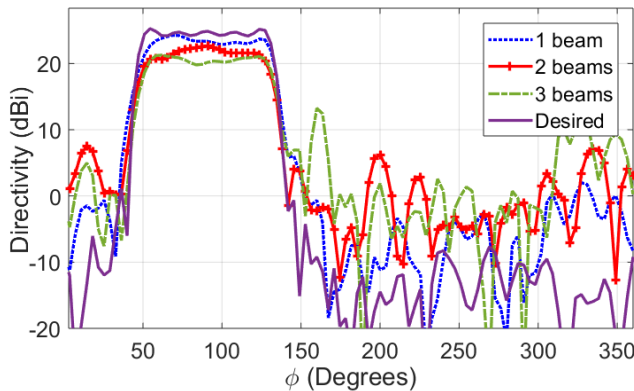


Fig. 11. Comparison between the radiation patterns for MTS radiating an azimuthally symmetric beam ($Q = 1$, $Q = 2$ and $Q = 3$).

first feed. The desired radiation pattern can then be written for the first excitation as $F_{TE} = \cos 4\phi - j \sin 4\phi$ and $F_{TM} = -\sin 4\phi - j \cos 4\phi$. For the second excitation, one needs $F_{TE} = -\cos 4\phi - j \sin 4\phi$ and $F_{TM} = \sin 4\phi - j \cos 4\phi$ in the targeted direction. This beam does not satisfy the symmetry required to apply the method presented in Section III-A. The synthesis has, therefore, been carried out with the equations stacking method described in Section III-B.

We now analyze the impact of iterating over the invisible current spectrum, as explained in Section III-B. Fig. 12 represents the obtained impedance modulations. Fig. 13 shows the simulated embedded element patterns, corresponding to

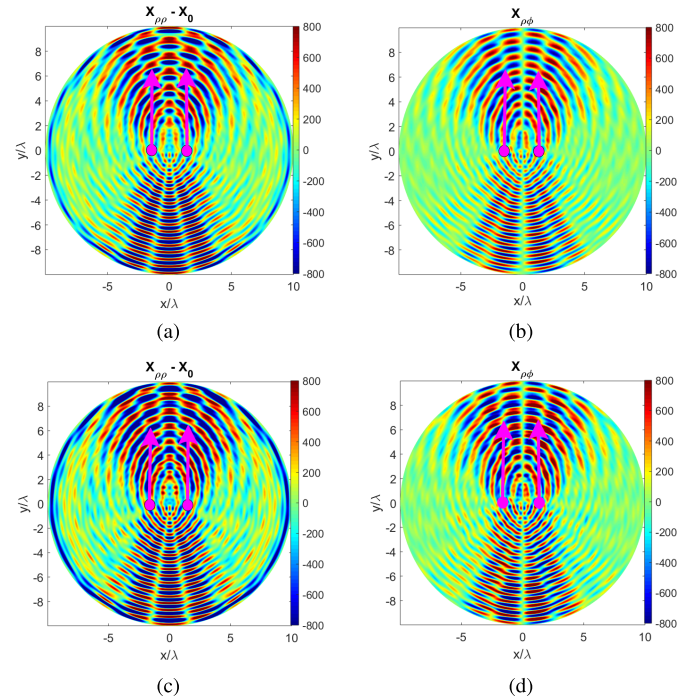


Fig. 12. Modulated sheet impedance for an MTS antenna radiating two azimuthal beams at $\theta = 30^\circ$ and $\phi \in [67.5^\circ, 112.5^\circ]$ with opposite polarizations. The dots represent the sources location. Synthesis based on the method described in Section III-B. (a) $X_{\rho\rho} - X_0$ at iteration 0. (b) $X_{\rho\phi}$ at iteration 0. (c) $X_{\rho\rho} - X_0$ at iteration 1. (d) $X_{\rho\phi}$ at iteration 1.

each excitation taken separately. The results obtained without iteration is compared to those obtained after one iteration. One can see a slight improvement on the radiation pattern. As observed, a good cross-polar level has been obtained after one iteration. The achieved aperture efficiency (computed with the desired radiation pattern) is near 44%. It is important to stress that the iteration process is not necessarily stable, i.e., it may sometimes lead to undesired amplification of the modulation depth after several iterations. The authors recommend two iteration steps and selection of the best performance among the three obtained results.

C. MTS Design for Beam Scanning

The goal of this section consists of numerically demonstrating the possibility of beam scanning using multifed phased MTSS. The used parameters (frequency, substrate, radius, feeding points, etc.) are the same as in the previous section. As opposed to the dual-pol configuration, here we want to generate two embedded element patterns with the same amplitude and polarization (TM) but with different phase progressions. For the first excitation, the phase linearly increases w.r.t. ϕ and covers a phase range of π radian. For the second excitation, the phase linearly decreases, with the same phase range. Exciting the first feed, the desired radiation pattern is then given as $F_{TE} = 0$ and $F_{TM} = \sin 4\phi - j \cos 4\phi$ in the targeted direction. For the second excitation, we want $F_{TE} = 0$ and $F_{TM} = -\sin 4\phi - j \cos 4\phi$. We now excite the two feed points with the same magnitude and a relative phase ψ . The global radiation pattern can then be written as

$$\mathbf{F}(\theta, \phi) = U_\phi \hat{p} (e^{jk\phi} + e^{j\psi} e^{-jk\phi}) \quad (13)$$

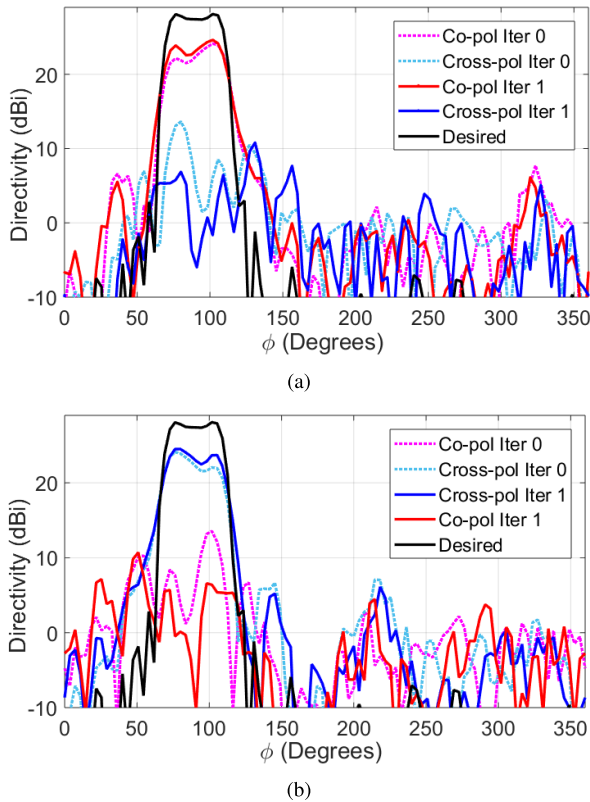


Fig. 13. Comparison between the embedded element patterns obtained at iteration 0 with those obtained after a first iteration along the cone $\theta = 30^\circ$. (a) Feed 1. (b) Feed 2.

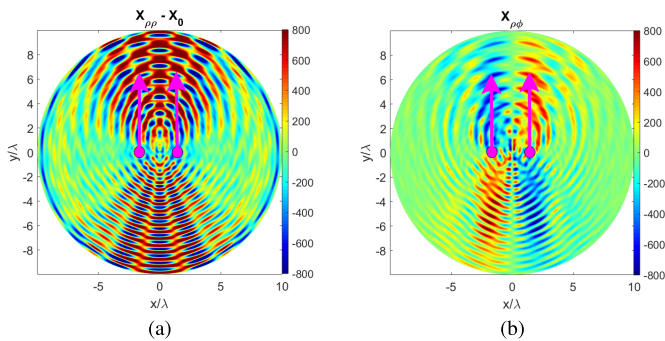


Fig. 14. Modulated sheet impedance for an MTS antenna radiating two circularly polarized azimuthal beams at $\theta = 30^\circ$ and $\phi \in [67.5^\circ, 112.5^\circ]$ with different phase progression. The dots represent the source locations. The synthesis is based on the method described in Section III-B. (a) $X_{\rho\rho} - X_0$. (b) $X_{\rho\phi}$.

where the window U_ϕ is equal to one for $\theta = 30^\circ$ and $\phi \in [67.5^\circ, 112.5^\circ]$ and 0 elsewhere. \hat{p} is the TM unit vector polarization. $k = (\pi/\Delta\phi)$, with $\Delta\phi = (112.5^\circ - 67.5^\circ)\pi/180$. The expression between brackets in (13) can be interpreted as an array factor and can be rewritten as $e^{j\psi/2} \cos(k\phi - \psi/2)$, which means that the antenna beam is linearly polarized with a maximum directivity at $\phi = -\psi/(2k)$. Therefore, one can achieve continuous azimuthal scanning by varying the phase ψ of excitation at one of the two feed points. Fig. 14 shows the obtained impedance modulation. Fig. 15 illustrates the beam-scanning capability. One can see that a beam scanning

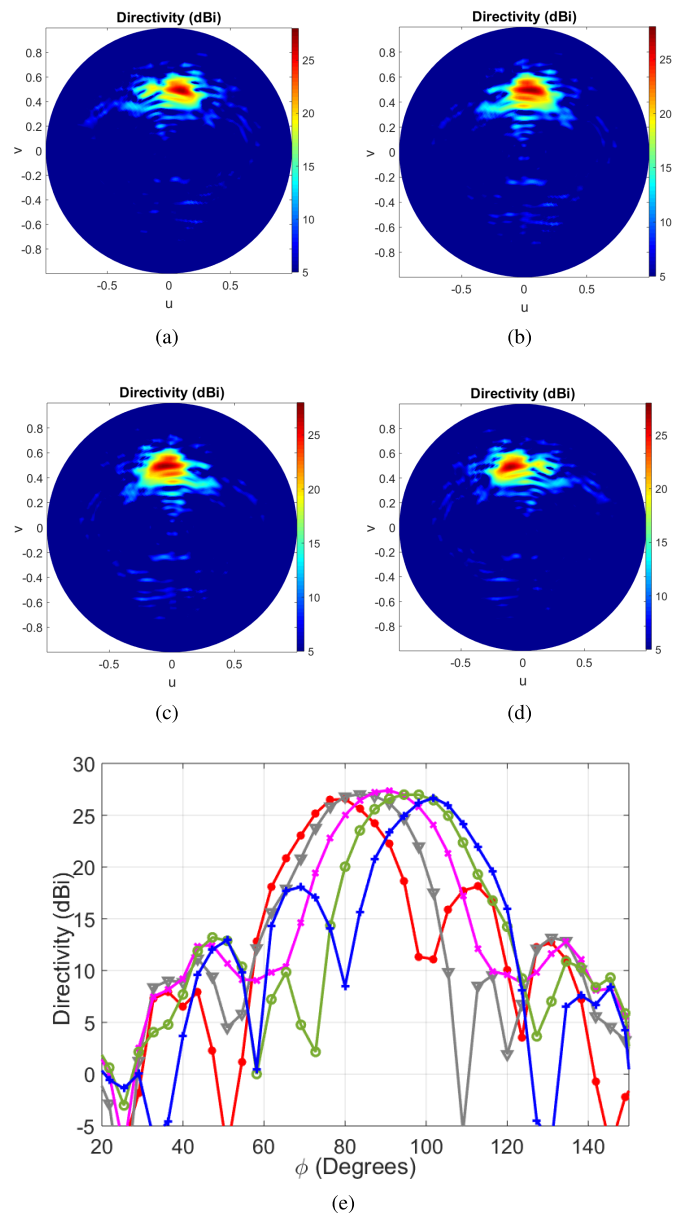


Fig. 15. Beam-scanning capabilities of a two-feed MTS antenna. (a)–(d) Illustration in the u - v plane for different values of ψ . (e) Illustration along the cone $\theta = 30^\circ$ for different values of ψ equally spaced in the range $[0, 2\pi]$.

over about 20° has been achieved. The sidelobe level is quite high. Indeed, when the array is scanned, neighboring lobes of $\cos(k\phi - \psi/2)$ in the array factor start to enter into the window U_ϕ . For larger scan angles, the next lobe of $\cos(k\phi - \psi/2)$ appears as important sidelobes. Since there is only one degree of freedom, the method allows a beam scanning over a 3 dB beamwidth only. One can choose independently the beamwidth based on the width of the radiation pattern associated with each excitation.

V. CONCLUSION

We have presented the generation of multishaped beams with MTS antennas. The proposed methods are based on the EFIE discretization with FBBFs. In particular, we discussed two techniques. The first one relies on the azimuthal symmetry

of the impedance to naturally impose an azimuthal symmetry on the radiation pattern. The second method consists of over-constraining the system of equations and can be used for more general multibeam. However, this approach is more time and memory consuming than the first one. Finally, we have proved that a proper control of the amplitude, phase, and polarization of the radiation pattern can allow continuous beam steering by phasing the MTS at multiple feed points: two points and azimuthal beam scanning so far. To the best of our knowledge, it is the first time that phased MTS antennas has been proposed for beam scanning. Further research should allow one to increase the number of feeds in order to improve the scanning capability, for instance, obtaining the same scan range with a narrower beam. Another point deserving further attention concerns the *a priori* estimation of the antenna near-field. In this article, the near-field corresponding to the average impedance has first been used and we have iterated over this first estimation to slightly improve the results. However, a better *a priori* estimation of the near-field taking into account the desired multibeam effect may allow one to achieve better performance.

REFERENCES

- [1] K. Bahadori and Y. Rahmat-Samii, "An array-compensated spherical reflector antenna for a very large number of scanned beams," *IEEE Trans. Antennas Propag.*, vol. 53, no. 11, pp. 3547–3555, Nov. 2005.
- [2] A. Garcia-Pino *et al.*, "Bifocal reflector antenna for a standoff radar imaging system with enhanced field of view," *IEEE Trans. Antennas Propag.*, vol. 62, no. 10, pp. 4997–5006, Oct. 2014.
- [3] M. K. Saleem, H. Vettikaladi, M. A. S. Alkanhal, and M. Himdi, "Lens antenna for wide angle beam scanning at 79 GHz for automotive short range radar applications," *IEEE Trans. Antennas Propag.*, vol. 65, no. 4, pp. 2041–2046, Apr. 2017.
- [4] W. Hong *et al.*, "Multibeam antenna technologies for 5G wireless communications," *IEEE Trans. Antennas Propag.*, vol. 65, no. 12, pp. 6231–6249, Dec. 2017.
- [5] O. Quevedo-Teruel, M. Ebrahimpouri, and F. Ghasemifard, "Lens antennas for 5G communications systems," *IEEE Commun. Mag.*, vol. 56, no. 7, pp. 36–41, Jul. 2018.
- [6] K. Kibaroglu, M. Sayginer, and G. M. Rebeiz, "A low-cost scalable 32-element 28-GHz phased array transceiver for 5G communication links based on a 2×2 beamformer flip-chip unit cell," *IEEE J. Solid-State Circuits*, vol. 53, no. 5, pp. 1260–1274, May 2018.
- [7] O. Quevedo-Teruel, J. Miao, M. Mattsson, A. Algaba-Brazalez, M. Johansson, and L. Manholm, "Glide-symmetric fully metallic Luneburg lens for 5G communications at ka-band," *IEEE Antennas Wireless Propag. Lett.*, vol. 17, no. 9, pp. 1588–1592, Sep. 2018.
- [8] A. Jacomb-Hood and E. Lier, "Multibeam active phased arrays for communications satellites," *IEEE Microw. Mag.*, vol. 1, no. 4, pp. 40–47, Dec. 2000.
- [9] G. Han, B. Du, W. Wu, and B. Yang, "A novel hybrid phased array antenna for satellite communication on-the-move in Ku-band," *IEEE Trans. Antennas Propag.*, vol. 63, no. 4, pp. 1375–1383, Apr. 2015.
- [10] E. de Lera Acedo, N. Razavi-Ghods, N. Troop, N. Drought, and A. J. Faulkner, "SKALA, a log-periodic array antenna for the SKA-low instrument: Design, simulations, tests and system considerations," *Experim. Astron.*, vol. 39, no. 3, pp. 567–594, 2015.
- [11] G. W. Kant, P. D. Patel, S. J. Wijnholds, M. Ruiter, and E. van der Wal, "EMBRACE: A multi-beam 20,000-element radio astronomical phased array antenna demonstrator," *IEEE Trans. Antennas Propag.*, vol. 59, no. 6, pp. 1990–2003, Jun. 2011.
- [12] K. F. Warnick, R. Maaskant, M. V. Ivashina, D. B. Davidson, and B. D. Jeffs, "High-sensitivity phased array receivers for radio astronomy," *Proc. IEEE*, vol. 104, no. 3, pp. 607–622, Mar. 2016.
- [13] J. Costantine, Y. Tawk, S. E. Barbin, and C. G. Christodoulou, "Reconfigurable antennas: Design and applications," *Proc. IEEE*, vol. 103, no. 3, pp. 424–437, Mar. 2015.
- [14] G. Minatti, S. Maci, P. De Vita, A. Freni, and M. Sabbadini, "A circularly-polarized isoflux antenna based on anisotropic metasurface," *IEEE Trans. Antennas Propag.*, vol. 60, no. 11, pp. 4998–5009, Nov. 2012.
- [15] G. Minatti *et al.*, "Modulated metasurface antennas for space: Synthesis, analysis and realizations," *IEEE Trans. Antennas Propag.*, vol. 63, no. 4, pp. 1288–1300, Apr. 2014.
- [16] M. Li, S.-Q. Xiao, and D. F. Sievenpiper, "Polarization-insensitive holographic surfaces with broadside radiation," *IEEE Trans. Antennas Propag.*, vol. 64, no. 12, pp. 5272–5280, Dec. 2016.
- [17] B. B. Tierney and A. Grbic, "Arbitrary beam shaping using 1-D impedance surfaces supporting leaky waves," *IEEE Trans. Antennas Propag.*, vol. 63, no. 6, pp. 2439–2448, Jun. 2015.
- [18] G. Minatti, F. Caminita, E. Martini, M. Sabbadini, and S. Maci, "Synthesis of modulated-metasurface antennas with amplitude, phase, and polarization control," *IEEE Trans. Antennas Propag.*, vol. 64, no. 9, pp. 3907–3919, Sep. 2016.
- [19] M. Teniou, H. Roussel, N. Capet, G.-P. Piau, and M. Casaletti, "Implementation of radiating aperture field distribution using tensorial metasurfaces," *IEEE Trans. Antennas Propag.*, vol. 65, no. 11, pp. 5895–5907, Nov. 2017.
- [20] M. Bodehou, C. Craeye, E. Martini, and I. Huynen, "A quasi-direct method for the surface impedance design of modulated metasurface antennas," *IEEE Trans. Antennas Propag.*, vol. 67, no. 1, pp. 24–36, Jan. 2019.
- [21] M. Bodehou, C. Craeye, and I. Huynen, "Electric field integral equation-based synthesis of elliptical-domain metasurface antennas," *IEEE Trans. Antennas Propag.*, vol. 67, no. 2, pp. 1270–1274, Feb. 2019.
- [22] S. F. Mahmoud, Y. M. M. Antar, H. F. Hammad, and A. P. Freundorfer, "Theoretical considerations in the optimization of surface waves on a planar structure," *IEEE Trans. Antennas Propag.*, vol. 52, no. 8, pp. 2057–2063, Aug. 2004.
- [23] D. González-Ovejero, N. Chahat, R. Sauleau, G. Chattopadhyay, S. Maci, and M. Ettore, "Additive manufactured metal-only modulated metasurface antennas," *IEEE Trans. Antennas Propag.*, vol. 66, no. 11, pp. 6106–6114, Nov. 2018.
- [24] E. Martini, M. Mencagli, Jr., and S. Maci, "Metasurface transformation for surface wave control," *Philos. Trans. Roy. Soc. London A, Math. Phys. Sci.*, vol. 373, no. 2049, pp. 2992–3003, Jul. 2015.
- [25] A. M. Patel and A. Grbic, "Modeling and analysis of printed-circuit tensor impedance surfaces," *IEEE Trans. Antennas Propag.*, vol. 61, no. 1, pp. 211–220, Jan. 2013.
- [26] A. M. Patel and A. Grbic, "Effective surface impedance of a printed-circuit tensor impedance surface (PCTIS)," *IEEE Trans. Microw. Theory Techn.*, vol. 61, no. 4, pp. 1403–1413, Apr. 2013.
- [27] D. González-Ovejero, G. Minatti, G. Chattopadhyay, and S. Maci, "Multibeam by metasurface antennas," *IEEE Trans. Antennas Propag.*, vol. 65, no. 6, pp. 2923–2930, Jun. 2017.
- [28] G. Minatti, F. Caminita, E. Martini, and S. Maci, "Flat optics for leaky-waves on modulated metasurfaces: Adiabatic floquet-wave analysis," *IEEE Trans. Antennas Propag.*, vol. 64, no. 9, pp. 3896–3906, Sep. 2016.
- [29] M. A. Francavilla, E. Martini, S. Maci, and G. Vecchi, "On the numerical simulation of metasurfaces with impedance boundary condition integral equations," *IEEE Trans. Antennas Propag.*, vol. 63, no. 5, pp. 2153–2161, May 2015.
- [30] D. González-Ovejero and S. Maci, "Gaussian ring basis functions for the analysis of modulated metasurface antennas," *IEEE Trans. Antennas Propag.*, vol. 63, no. 9, pp. 3982–3993, Sep. 2015.
- [31] M. Bodehou, D. González-Ovejero, C. Craeye, and I. Huynen, "Method of moments simulation of modulated metasurface antennas with a set of orthogonal entire-domain basis functions," *IEEE Trans. Antennas Propag.*, vol. 67, no. 2, pp. 1119–1130, Feb. 2019.
- [32] A. Aghasi, H. Amindavar, E. L. Miller, and J. Rashed-Mohassel, "Flat-top footprint pattern synthesis through the design of arbitrary planar-shaped apertures," *IEEE Trans. Antennas Propag.*, vol. 58, no. 8, pp. 2539–2552, Aug. 2010.
- [33] M. Bodehou, C. Craeye, H. Bui-Van, and I. Huynen, "Fourier-bessel basis functions for the analysis of elliptical domain metasurface antennas," *IEEE Antennas Wireless Propag. Lett.*, vol. 17, no. 4, pp. 675–678, Apr. 2018.
- [34] S. Ramalingam, C. A. Balanis, C. R. Birtcher, and H. N. Shaman, "Polarization-diverse holographic metasurfaces," *IEEE Antennas Wireless Propag. Lett.*, vol. 18, no. 2, pp. 264–268, Feb. 2019.



Modeste Bodehou (S'16) was born in Cotonou, Benin, in 1992. He received the B.Sc. degree in engineering and the M.Sc. degree in electrical engineering (telecommunication) from the Royal Military Academy, Brussels, Belgium, in 2013 and 2015, respectively. He is currently pursuing the Ph.D. degree with the Microwave and Applied Electromagnetism Laboratory, Université catholique de Louvain, Louvain-la-Neuve, Belgium.

In 2015, he was with Quartier Major Housiau (Belgium Defense), Vilvoorde, Belgium, where he was involved in the framework of his application school on military communication systems. His current research interests include computational electromagnetics, antenna arrays, and metasurfaces.

Mr. Bodehou was a recipient of the Best Student Paper Award at the 13th European Conference on Antennas and Propagation, Krakow, Poland, 2019, the First Prize Student Paper Competition Award at the IEEE-MTT International Conference on Numerical Electromagnetic and Multiphysics Modeling and Optimization for RF, Microwave, and Terahertz Applications, Seville, Spain, 2017, and the AIA Price for the Best Engineering Master Thesis Award from the Royal Military Academy, Brussels, Belgium, 2015.



Enrica Martini (S'98–M'02–SM'13) was born in Spilimbergo (PN), Italy, in 1973. She received the Laurea degree (*cum laude*) in telecommunication engineering from the University of Florence, Florence, Italy, in 1998, where she worked under a one-year research grant from Alenia Aerospazio Company, Rome, Italy, until 1999, the Ph.D. degree in informatics and telecommunications from the University of Florence, in 2002, and the Ph.D. degree in electronics from the University of Nice-Sophia Antipolis, Nice, France, in 2002, under joint supervision.

In 2002, she was appointed as a Research Associate with the University of Siena, Siena, Italy. She joined the Electromagnetic Systems Section of the Ørsted-DTU Department until 2007. From 2007 to 2017, she was a Post-Doctoral Fellow with the University of Siena. From 2016 to 2018, she was the CEO of the start-up Wave Up Srl, Siena, that she co-founded in 2012. She is currently an Assistant Professor with the University of Siena. Her current research interests include metasurfaces, metamaterial characterization, electromagnetic scattering, antenna measurements, finite-element methods, and tropospheric propagation.

Dr. Martini was a co-recipient of the 2016 Schelkunoff Transactions Prize Paper Award and the Best Paper Award in Antenna Design and Applications at the 11th European Conference on Antennas and Propagation. In 2005, she received the Hans Christian Ørsted Postdoctoral Fellowship from the Technical University of Denmark, Lyngby, Denmark.



Stefano Maci (M'92–SM'99–F'04) received the Laurea degree (*cum laude*) in electronics engineering from the University of Florence, Florence, Italy, in 1987.

In 2004, he was the Founder of the European School of Antennas, a postgraduate school that presently comprises 30 courses on antennas, propagation, electromagnetic theory, and computational electromagnetics, with 150 teachers from 15 countries. From 2004 to 2007, he was the WP Leader of the Antenna Center of Excellence (ACE; FP6-EU)

and the International Coordinator of the 24-institution consortium of a Marie Curie Action (FP6) from 2007 to 2010. Since 2010, he has been a Principal Investigator of six cooperative projects financed by the European Space Agency. He has been the Director of the University of Siena's Ph.D. Program in information engineering and mathematics from 2008 to 2015 and a member of the National Italian Committee for Qualification to Professor from 2013 to 2015. He was a Co-Founder of two spin-off companies. He is currently the Director of the consortium FORESEEN, which currently consists of 48 European institutions and a Principal Investigator of the Future Emerging Technology project Nanoarchitectonics of the 8th EU Framework program. Since 1997, he has been a Professor with the University of Siena, Siena, Italy. He has coauthored over 160 articles published in international journals, among which 100 are in IEEE journals, 14 book chapters, and about 400 articles in proceedings of international conferences. These articles have received around 6800 citations. His current research interests include high-frequency and beam representation methods, computational electromagnetics, large phased arrays, planar antennas, reflector antennas and feeds, metamaterials, and metasurfaces.

Prof. Maci was a former member of the IEEE AP-S AdCom, EurAAP Board of Directors, and Antennas and Propagation Executive Board of the Institution of Engineering and Technology, U.K. He has been a member of the Technical Advisory Board of 11 international conferences and the Review Board of six International Journals since 2000. He was a recipient of the European Association on Antennas and Propagation (EurAAP) Award in 2014, the Sergei A. Schelkunoff Transactions Prize Paper Award, and the Chen-To Tai Distinguished Educator Award from the IEEE Antennas and Propagation Society (IEEE AP-S) in 2016. He has organized 25 special sessions in international conferences and held 10 short courses in the IEEE AP-S Symposia about metamaterials, antennas, and computational electromagnetics. He is a Distinguished Lecturer of the IEEE AP-S and EuRAAP. He was the Chair of the Award Committee of IEEE AP-S. He was an Associate Editor of the IEEE TRANSACTIONS ON ANTENNAS AND PROPAGATION.



Isabelle Huynen (M'96–SM'06) received the Ph.D. degree in applied sciences from the Université catholique de Louvain (UCLouvain), Louvain-la-Neuve, Belgium, in 1994.

Since 1999, she has been with FRS-FRNS, Bruxelles, Belgium. She is currently the Research Director and a part-time Professor with UCLouvain. Her current research interests cover nanotechnology, nanodevices and nanomaterials for microwave and millimeter wave applications, including metamaterials, antennas, and absorbers.



Christophe Craeye (M'98–SM'11) was born in Ronse, Belgium, in 1971. He received the B.Phil. degree, the M.Sc. degree in electrical engineering, and the Ph.D. degree in applied sciences from the Université catholique de Louvain (UCLouvain), Louvain-la-Neuve, Belgium, in 1994, 1994, and 1998, respectively.

From 1994 to 1999, he was a Teaching Assistant with UCLouvain, where he was involved in the research on the radar signature of the sea surface perturbed by rain, in collaboration with NASA and ESA. From 1999 to 2001, he was a Post-Doctoral Researcher with the Eindhoven University of Technology, Eindhoven, The Netherlands, where he was involved in wideband phased arrays devoted to the square kilometer array radio telescope. In this framework, he was also with the University of Massachusetts, Amherst, MA, USA, in 1999 and with the Netherlands Institute for Research in Astronomy, Dwingeloo, The Netherlands, in 2001. In 2002, he started an antenna research activity with UCLouvain, where he is currently a Professor. He was with the Astrophysics and Detectors Group, University of Cambridge, Cambridge, U.K., in 2011. His current research is funded by Région Wallonne, European Commission, ESA, FNRS, and UCLouvain. His current research interests include finite antenna arrays, wideband antennas, small antennas, metamaterials, and numerical methods for fields in periodic media, with applications to communication and sensing systems.

Dr. Craeye was a recipient of the 2005–2008 Georges Vanderlinden Prize from the Belgian Royal Academy of Sciences in 2009. He served as an Associate Editor for the IEEE TRANSACTIONS ON ANTENNAS AND PROPAGATION and the IEEE ANTENNAS AND WIRELESS PROPAGATION LETTERS from 2011 to 2017.